EFFECTS OF STRUCTURAL MATERIALS ON BP/CP UNCERTAINTY STUDIES FOR RFSP-IST MODELLING OF WOLSONG CANDU 6 REACTORS

Dai-Hai Chung[1*], Hyung-Jin Kim[1] and Sung-Min Kim[2]
[1]Atomic Creative Technology Co., Ltd., Daejeon, Korea
[2]Korea Hydro and Nuclear Power Co., Ltd., Daejeon, Korea
[*]*Corresponding author: dhchung@actbest.com*

Abstract

A study has been carried out to gain a picture and some quantitative evaluations of the structural material mesh spacing layout effects of Wolsong CANDU 6 reactors by using the WIMS/DRAGON/RFSP-IST code system. The newly updated code system has been validated to some extents by comparing the Phase-B pre-simulation results of Wolsong Unit 1 against the previously acquired Phase-B commissioning test measurements of Wolsong Units 1,2,3,4. The code validation efforts resulted in the conclusions that the newly adopted code system could be used for the operational support of Wolsong CANDU 6 reactors. As an ongoing striving for the improvement of safe and economic operation of the reactors, a project on BP/CP uncertainty analysis with respect to the WIMS/DRAGON/RFSP-IST code system is planned. The results obtained in the present study strongly suggest that the effects of mesh spacing layouts of structural materials could be used as an important parameter to help grasp a more realistic glance on the overall off-line flux mapping errors that contribute to BP/CP uncertainties.

1. Introduction

The Wolsong-1 CANDU 6 reactor (W-1) is currently undergoing a major refurbishment project including replacement of the pressure tube. The safety analysis and Phase-B pre-simulations of the reactor have been completed for the licensing submission and restart tests by using the newly adopted code system WIMS/DRAGON/RFSP-IST (Refs. 1,2,3) in replacement of the previous PPV/MULTICELL/RFSP (Refs. 4,5) code suite. After the refurbishment, the reactor is due to be operated based upon the Improved Technical Specifications (ITS) derived from the Improved Standard Technical Specifications (ISTS) (Ref. 6), that are currently under the review of the domestic regulatory body, Korea Institute of Nuclear Safety (KINS).

The operation of W-1,2,3,4 is currently relying on the AECL produced single channel formalism for the bundle and channel power allowance limits. During the review process of ISTS, KINS has requested KHNP to evaluate BP/CP uncertainties based upon the 380 channel formalism. In other words, the BP/CP uncertainties will have to be assessed for all 380 channels individually. Thus, a study has been conducted in the presented paper as a preliminary attempt to accomplish grounding exercises that would be eventually useful to complement the entire BP/CP uncertainty analysis package.

For this purpose, the topic of mesh spacing layout with respect to the structural materials in the core is selected to figure out how this would affect the regional flux shape distributions. This conceptual approach to follow the flux shape changes under various circumstances, such as, like mesh spacing layout would represent a methodological consistency in line with the estimate of off-line flux mapping errors for CANDU 6 reactors.

The study has been carried out with the exclusive use of WIMS/DRAGON/RFSP-IST as it would be the official code system for W-1,2,3,4 reactors in a foreseeable future. Special emphasis has been placed to the meaning and importance of the DRAGON-IST code generated incremental cross sections that represent the structural materials as the theory implemented in the code reflects more rigorous mathematics and physics modelling practices based upon the collision probability theory, which would be in contrast to the previously used MULTICELL incremental cross sections that are derived based upon the reaction rate average method using the diffusion theory.

The qualification of the WIMS/DRAGON/RFSP-IST code system has been elsewhere (Ref. 7) justified for the use in context of operational support of Wolsong CANDU 6 reactors. Thus, the results obtained here using the code system would also be legitimate ones to support the forthcoming BP/CP uncertainty analysis.

In the following, the methodological approach to layout mesh spacings will be discussed along with the associated importance with respect to the reaction rates of each individual structural material. After that, the time-average model used for the simulations will be briefly presented. Finally, the results obtained based upon the various layout of mesh spacings will be presented and compared against each others and discussed followed by some conclusions.

2. Background of Numerical Implications of Diffusion Theory Finite Difference Scheme

The two-energy-group neutron diffusion equations adopted in RFSP-IST are numerically solved by using the finite differencing representation of the leakage terms that are approximated by parabolic fitting of the flux distribution functions. In theory, this finite difference numerical scheme generated solutions of the flux distributions within the domain of interest will converge to exact solutions with second order convergence rate as the spatial mesh sizes used to approximate the diffusion terms become smaller. However, this theoretical expectation is ruined due to the presence of heterogeneities associated with the neutron absorbing materials, such as, fuel, reactivity devices and its supporting structural components in the core, and some of them, e.g., steels, are characterized by strong neutron absorptions.

Furthermore, in the regions where the structural materials are sitting in the bottom of core the diffusion theory fails to adequately represent neutron transport phenomena and it is a very difficult task to derive qualified model to represent such a situation precisely, which is usually replaced by incremental cross sections being imposed on the diffusion theory compatible macroscopic cross sections. Thus, it would be an interesting subject to investigate the implications of structural material incremental cross sections in conjunction with the RFSP-IST numerical solutions of the diffusion equations.

The top-to-bottom tilt of flux distribution in CANDU reactor core has been well known since the inception of CANDU power reactors. It would be a general consensus that the flux tilt phenomena in large reactor core with abundant volume of moderator like in CANDU power reactors justify themselves to claim the understanding of consequences arising from the flux tilt in-depth to have realistic answers related to many problems, among which the issues, that are related directly with the flux distribution, of long-term fuel management strategies, neutron leakages across the core, xenon oscillations, control of zone powers and uncertainties in maximum bundle and channel power allowance limits as well as neutronic trip settings should be considered as practically important.

The incremental cross sections generated by using DRAGON-IST along with the WIMS-IST produced fuel properties are the ones that are invited here to help grasp an updated glance of the effects of structural materials in conjunction with the mesh spacing layout in RFSP-IST core model.

3. Incremental Cross Sections and Reaction Rates of Structural Materials

The typical CANDU 6 RFSP-IST model shows 497 reactivity device related inputs in *DATA module, which include the reactivity devices themselves and the corresponding guide tubes as well as the associated structural materials. The input is specified with the so-called device name and type, respectively. The device type is characterized by its incremental cross sections. These incremental cross sections are added to the two-energy group macroscopic cross sections to solve numerically the diffusion equations. In doing so, the incremental cross sections are smeared over finite difference mesh volume by applying the volumetric ratio of the partial volume of a reactivity device that is contained in a mesh volume to the mesh volume unless the six surfaces of the device parallelepiped do not exactly coincide with the six surfaces of the mesh parallelepiped. This practice is bound with the compromising negligence of the originally intended effects of reactivity device modelling itself and its associated other materials being modelled by using incremental cross sections. Since the number of reactivity devices themselves and its associated material boundaries that do not coincide with the finite difference mesh volume boundaries in RFSP-IST core model exceedingly exist, the smearing effect of incremental cross sections are certainly reflected in the flux distributions that are obtained by RFSP-IST simulations.

The core model to simulate steady-state operations is characterized by the loading of 21 adjuster rods (ADJs) and 14 liquid zone controllers (LZCs). Beside these two major reactivity devices, there are mechanical control absorbers (MCAs) and shutoff rods (SORs). The MCAs and SORs are hung in the reactivity mechanism deck out of the core during steady-state operations.

Table 1a Thermal Absorption Incremental Cross Sections and Reaction Rates of Structural Materials
($\Delta\Sigma_{a,2}$,[cm^{-1}], Reaction Rate (RR) = $\Phi\Delta\Sigma_{a,2}V$ [n/s] with $\Phi=1$)

	ADJ		MCA		SOR		ZCR	
	$\Delta\Sigma_{a,2}$	RR	$\Delta\Sigma_{a,2}$	RR	$\Delta\Sigma_{a,2}$	RR	$\Delta\Sigma_{a,2}$	RR
Nuts (NUT)	3.0852E-03	2.3292E+02	4.6886E-03	6.7421E+01	4.6886E-03	4.7194E+02	4.2082E-03	1.0167E+02
Brackets and Locators (BL)	2.1971E-03	1.2472E+03	2.1971E-03	2.3757E+02	2.1971E-03	1.6630E+03	2.1971E-03	3.5635E+02
Tension Springs (TS)	2.4984E-03	1.7005E+03	3.7183E-03	4.3153E+02	3.7183E-03	3.0207E+03	3.3111E-03	4.1333E+02
	Sum	3.1807E+03	Sum	7.3652E+02	Sum	5.1556E+03	Sum	8.7135E+02

Table 1b Thermal Absorption Incremental Cross Sections and Reaction Rates of Structural Materials
($\Delta\Sigma_{a,2}$,[cm^{-1}], Reaction Rate (RR) = $\Phi\Delta\Sigma_{a,2}V$ [n/s] with $\Phi=1$)

Moderator Injection Nozzles		Liquid Poison Injection BL		Vertical Flux Detector BL		Horizon Flux Detector BL		Sum
$\Delta\Sigma_{a,2}$	RR	$\Delta\Sigma_{a,2}$	RR	$\Delta\Sigma_{a,2}$	RR	$\Delta\Sigma_{a,2}$	RR	RR
3.1149E-03	6.3484E+02	2.1971E-03	3.5635E+02	2.1971E-03	1.5442E+03	2.1971E-03	5.3453E+02	3.0699E+03

Table 2 Thermal Absorption Incremental Cross Sections and Reaction Rates of Adjuster Rods
($\Delta\Sigma_{a,2}$,[cm^{-1}], Reaction Rate (RR) = $\Phi\Delta\Sigma_{a,2}V$ [n/s] with $\Phi=1$)

A-INNER		A-OUTER		B-TYPE		C-INNER		C-OUTER		D-TYPE		SUM
$\Delta\Sigma_{a,2}$	RR	$\Delta\Sigma_{a,2}$	RR	$\Delta\Sigma_{a,2}$	RR	$\Delta\Sigma_{a,2}$	RR	$\Delta\Sigma_{a,2}$	RR	$\Delta\Sigma_{a,2}$	RR	RR
6.0728E-04	4.4208E+02	5.2437E-04	3.8173E+02	8.9705E-04	2.6121E+03	8.1864E-04	1.1919E+03	3.6302E-04	5.2854E+02	5.0876E-04	4.9381E+02	5.6502E+03

The thermal absorption incremental cross sections of ADJs range between about 3.63E-04 cm^{-1} and 8.97E-04 cm^{-1} according to the grade of stainless steel that are in place as neutron absorbing materials of ADJs. The thermal absorption incremental cross sections of the guide tubes associated with flux detector assemblies, MCAs, SORs, ADJs, LZCs and poison injectors as well as ADJ support cables and bars range between 6.13E-06 cm^{-1} and 3.63E-05 cm^{-1}, and these materials can be treated as lightly neutron absorbing, e.g., in comparison to stainless steel of ADJs, so that the corresponding guide tubes, cables and bars are not considered in laying out mesh spacings to represent exactly their geometric boundaries. In other words, the incremental cross sections of these lightly neutron absorbing materials are smeared over the finite difference mesh volumes whenever their boundaries are not coincident with the mesh boundaries.

The thermal absorption incremental cross sections of the rest of the structural materials are summarized in Tables 1a and 1b along with the corresponding reaction rates. The reaction rates are calculated by applying flat fluxes with unity in magnitude.

For the comparison purposes, the similar quantities as shown in Tables 1a and 1b are also given for the adjuster rods in Table 2.

Note that the thermal absorption incremental reaction rate of the SOR structural materials, 5.1556E+03 n/s, is about ~91% of that of all the adjuster rods. The total sum of the thermal absorption incremental reaction rates of all the structural materials as listed in Tables 1a and 1b is 1.3014E+04 n/s, which is about ~130% more than that of all the adjuster rods. However, the actual flux levels associated with the above-mentioned structural materials would be in reality lower than the flux levels at the adjuster rod locations in the core. Nevertheless, the importance and significance of structural material mesh spacing layouts in the RFSP-IST core model and its conveying consequences are clearly vindicated through the observations taken here.

4. Mesh Spacing Layout – Reference Model

The distance of the coordinate axes in x- and y-directions of the finite difference RFSP-IST CANDU 6 core model spans 0-765.7 cm, respectively. The length of axial dimension is 12 bundles x 49.53 cm/bundle = 594.36 cm on z-axis. In x-y plane the meshes are firstly laid out with a uniform mesh size of 28.575 cm that is equivalent to the lattice pitch of WIMS-IST lattice cell model. This leads to 765.7 - 26x28.575 = 22.75 cm, from which the first and last mesh sizes at the left and right as well as the top and bottom boundaries become 22.75/2 = 11.375 cm, respectively. Thus, the basic mesh layout becomes 28x28x12 mesh intervals in x-, y- and z-directions, which warrants at least one mesh line coincident with the lattice cell boundaries in the core region loaded with fuel bundles, respectively.

Further mesh lines onto the basic mesh layout (28x28x12) are added by creating mesh line at the boundaries of ADJs, MCAs and SORs, respectively. In order to make also useful for the time-dependent simulation of SDS2 poison injections into the moderator system, the mesh lines are again complemented to match the boundaries of liquid poison mixing propagations with time in the moderator volume. Accounting all these considerations, the number of mesh intervals in x-, y- and z-directions become 48x40x40, respectively (see Table 3). This model can be used both for steady-state and SDS1/2 associated transient simulations without changing the mesh layouts and will be called as standard model, Model S. Note that in this model six surface boundaries of parallelepiped model of the structural materials are not considered.

Finally, the number of mesh intervals in x- and y-directions increase to 60x98 when all the surface boundaries of parallelepiped model of the structural materials that are not coincident with the existing mesh lines of the standard model accounted for. The z-direction mesh spacing number would have increased from 40 to 80 if all the axial surface boundaries of parallelepiped model of the structural materials that are not coincident with the existing mesh lines of the standard model in z-direction accounted for. However, any increase of mesh intervals against the standard model in z-direction could not be absorbed due to the limited feature of RFSP-IST. However, this limitation would not pose as significant errors as in the case of y-direction structural material mesh spacing layouts due to the symmetric location of structural materials in the axial direction, so that some errors might cancel out each other, whereas in y-direction the structural materials are mostly positioned in the bottom region of core.

The model with mesh intervals of 60x98x40 will be called as the reference model, Model R, and the corresponding RFSP-IST simulations will also be called as the reference simulations. Two and thirteen mesh intervals in x- and y-direction have mesh sizes smaller than 1 cm, respectively, and no attempt has been made to consolidate these mesh intervals with the neighbouring mesh intervals, so that the mesh sizes would become larger and the number of mesh intervals would reduce, in order to retain the completeness of the structural mesh spacing layouts.

Table 3 Mesh Spacing Distribution of RFSP-IST Standard Model (48x40x40)
(Mesh Sizes Are in Centimetres)

X-Direction		Y-Direction		Z-Direction	
(1)	0.0000	(1)	0.0000	(1)	0.0000
(2)-47)	11.3750	(2)-(39)	11.3750	(2)-(39)	49.5300
(3)-46)	28.5750	(3)-(38)	28.5750	(3)-(38)	47.6500
(7)-42)	14.2875	(4)-(37)	14.2875	(4)-(37)	1.8800
(48)	0.0000	(6)-(9)	28.5750	(5)-(36)	16.9100
		(16)-(16)	28.5750	(6)-(35)	26.2100
		(19)-(22)	28.5750	(7)-(34)	5.0000
		(25)-(25)	28.5750	(8)-(33)	1.4100
		(32)-(35)	28.5750	(9)-(32)	17.3800
		(40)	0.0000	(10)-(31)	6.2100
				(11)-(30)	20.2350
				(12)-(29)	5.7050
				(13)-(28)	24.0600
				(14)-(27)	10.0000
				(15)-(26)	9.76500
				(16)-(25)	5.70500
				(17)-(24)	4.2100
				(18)-(23)	20.5550
				(19)-(22)	9.7650
				(20)-(21)	15.0000
				(40)	0.0000

5. Mesh Spacing Layout – Reduced Mesh Line Models

Further models with reduced mesh lines whose numbers are less than the numbers of the reference model mesh lines are set up for the purpose of studying the effects of structural material mesh layouts. The guidelines applied to in creating these models are summarized in Table 4 along with the reference and standard models, Models R,S.

Two sets of models are considered, namely, the first one, Models A-D, showing the change in y-direction mesh line numbers while the mesh line numbers in x- and z-directions are held same as in the case of the reference model, and the second one, Models E-G,S, having the same mesh line numbers for y- and z-directions as compared to Models A-D but the mesh line numbers in x-direction are reduced to 48.

The closest model compared to the reference model, Model R, is Model A, in which the y-direction mesh line numbers are reduced from 98 to 92. Out of six mesh lines removed, two mesh lines correspond to the upper boundaries of the LZC unit assemblies and the rest represents the LZC structural materials.

Note that the selection of removing the mesh lines associated with a certain type of the structural materials is more or less intuitively made at this stage. However, the process of selecting a certain type of the structural material and to remove the associated mesh lines from model remains as a subject of further study because the results obtained with different removal pattern of the structural material associated mesh lines from model would convey different consequences in context of flux distributions in the core.

Table 4 Model Classifications Based Upon Structural Material Mesh Spacing Layouts
(x,y = x- and/or y-direction mesh lines are retained in model, respectively)

Model Type#	Mesh Layout	SOR	MCA	ADJ	ZCR*	MOD-INJ	LPI-BL	HFD-BL	VFD-BL
R	60x98x40	x, y	x, y	x, y	x, y	x, y	x, y	x, y	x, y
A	60x92x40	x, y	x, y	x, y	x	x, y	x, y	x, y	x, y
B	60x81x40	x, y	x, y	x, y	x	x	x	x	x
C	60x64x40	x, y	x	x	x	x	x	x	x
D	60x40x40	x	x	x	x	x	x	x	x
E	48x92x40	x, y	x, y	x, y	x	y	y	y	x, y
F	48x81x40	x, y	x, y	x, y	x				x
G	48x64x40	x, y	x	x	x				x
S	48x40x40	x	x	x	x				x

Model types R and S stand for the reference and the standard models, respectively.
* Two mesh lines representing the upper boundaries of ZCR (LZC) unit assemblies are included.

Note that for Models E-G,S the mesh lines removed in x-direction are only for MOD-INJ, LPI-BL and HFD-BL. The mesh lines for the rest of the structural materials in x-direction are already coincident with one of the existing mesh lines of the standard model, Model S, (see Table 3) so that there is no need for the consideration of these structural materials whether or not the removal of mesh lines in x-direction would change the mesh spacing layouts as in the case of y-direction mesh spacing layouts.

6. Time-Average Model

For the study of the effects of structural material mesh spacing layouts, a usual time-average model is used. In Table 5 the relevant WIMS-IST input parameter values are listed which would normally correspond to CANDU 6 reactor operating conditions and are used for design and safety analysis. The uniform fuel tables to be used for the time-average calculations are generated using WIMS Utilities programs (Ref. 8). The DRAGON incremental cross sections are generated (Refs. 2,9) based upon the operating conditions as listed in Table 5.

In Figure 1 the average exit burnup of eight burnup zones are displayed. The exit burnup distribution is intentionally tailored so that the excess system reactivity, $\Delta\rho = 1\text{-}1/k_{eff}$, yielded by using Model R becomes exactly nil. Note that the exit burnups used are not meant for the optimization of discharge burnups but merely serve as a sample for the study intended here. The time-average simulations are conducted by applying the standard bi-directional push-through eight bundle shift fuelling scheme and the flux convergence criterion is set to 1E-06.

Table 5 WIMS-IST Input Parameters for Time-Average Calculations

Parameter	Condition
Reactor Power [FP]	100%
W/g of Initial HE	33.4902
Coolant Temperature [ ]	288
Moderator Temperature [ ]	69
Fuel Temperature [ ]	687
Coolant Density [g/cm^3]	0.80786
Moderator Density [g/cm^3]	1.08509
NU Fuel Density [g/cm^3]	10.4919
Avg. Uranium Weight [kgU/BND]	19.13525
Coolant Purity [atom%]	99.000
Moderator Purity [atom%]	99.833

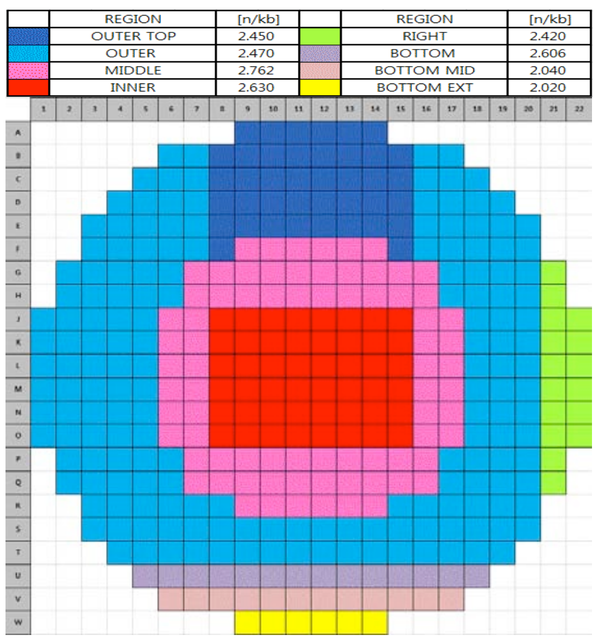

Figure 1 Time-Average Burnup Zones

7. Time-Average Simulation Results

The results of the time-average simulations carried out for Models R, A-G and S are summarized in Table 6. All the models reveal the same number of outer iteration loops, namely, 5, due to the same convergence criterion 1E-04 applied to the axial irradiation shape. The total number of flux iterations is dependent on the number of mesh volumes of the finite difference numerical schemes, and the behaviour of dependency shows a consistent pattern as the number of mesh volumes decreases. Note that Model R with the most number of mesh volumes, 60x98x40, shows about 39% more number of flux iterations compared to the case of Model S with the least number of mesh volumes, 48x40x40. Counting only the mesh rectangles in x-y planes without the dummy mesh volumes at the boundaries of the model, the ratio between the number of Model R and S mesh rectangles becomes (58x96)/(46x38) = ~3.18 whereas the ratio between the number of flux iterations is about ~1.39. This observation leads to a favourable thought that the increase of mesh lines due to structural materials would not pose concerns for the practical simulation exercises. Note that the increase of mesh lines due to the structural materials occurs in the narrowly limited volume of core bottom regions confined to the circumferential piece of calandria so that the actual increase of mesh volumes to be swept by the numerical algorithm of finite difference scheme becomes less.

Table 6 Results of Time-Average Simulations

	Model								
Result Type	**R**	**A**	**B**	**C**	**D**	**E**	**F**	**G**	**S**
# of Outer Iterations	5	5	5	5	5	5	5	5	5
Total # of Flux Iterations	4481	4263	3952	3492	3361	4275	3942	3390	3229
CPU (s)	92	84	66	49	37	79	62	45	33
$\Delta\rho$ (mk)	Nil	-0.004	-0.008	-0.032	-0.082	-0.060	-0.064	-0.088	-0.138
Max. BP-(kW)	806.37	806.54	807.73	807.01	807.67	799.42	802.26	801.53	802.52
Max. BP-Location	O-18/7	O-18/7	P-17/7	P-17/7	H-17/6	P-17/7	P-17/7	P-17/7	H-17/6
Max. CP-(MW)	6552.04	6553.35	6556.42	6558.80	6568.45	6503.88	6506.33	6508.61	6532.35
Max. CP-Location	N-17	N-17	N-17	N-17	M-18	N-17	N-17	N-17	H-15
Reactivity Decay Rate (mk/FPD)	-0.4662	-0.4662	-0.4663	-0.4665	-0.4670	-0.4664	-0.4665	-0.4667	-0.4671

The CPU time spent by RFSP-IST also displays a consistent pattern, and the CPU time ~92 s spent on Model R should be accepted as practically affordable computing time. The computer system used is X86-Based PC with the processor x86 Family 6 Model 15 Stepping 11 GenuineIntel ~2405Mhz. The system is operating under OS Microsoft Windows 7 Professional K, Version 6.1.7600.

The system excess reactivity, $\Delta\rho = 1\text{-}1/k_{eff}$, decrease with the reduction in the number of mesh volumes, however the changes should be considered as negligible for the practical applications. Note that the change in $\Delta\rho$ is not pronounced to lead to any concerns because it is a reaction rate average quantity integrated over the reactor volume so that some errors might have been cancelled out during the integration process.

The maximum bundle powers increase with the reduction in the number of mesh volumes in the model both for the grouping of Models R,A-D and Models E-G,S, respectively. In other words, the neglecting of the effects of structural material mesh spacing layouts results in the conservative estimate of maximum bundle powers. This observation is also valid for the case of maximum channel powers.

However, it comes to light that comparing Model A to E, B to F, C to G and D to S, respectively, the maximum bundle and channel powers become smaller and the effect of neglecting the structural materials MOD-INJ, LPI-BL and HFD-BL (see Table 4) for the mesh spacing layouts contributes to the hampering of conservatism. Thus, it is strongly suggested that the mesh lines in x-direction of the core model associated with the structural materials should be accounted for without any discarding.

The extreme off-differences of maximum bundle and channel powers occur between Model R and E. The off-differences are -0.86% and -0.74%, respectively. The locations of the maximum bundle and channel powers behave normally and some dislocations occur with the change of model, but they all remain within the central high power regions of the core.

Finally, the average reactivity decay rate (mk/FPD) behaves similarly to the case of $\Delta\rho$ but all the models practically yield the same values.

8. Zonal Flux Tilts

The results obtained from the time-average calculations by using Models R, A-G and S are further analysed in-depth in context of zonal flux distributions. The flux and power distribution in 14 zones, defined in usual way as it is associated with each corresponding LZC compartment, are the mandatory information to make various decisions during reactor operations, such as, e.g., fuel managements and shim operations. Furthermore, the snap-shot flux distributions with ripples are directly used to generate the fundamental mode of CANDU 6 off-line flux mapping system. Besides these, the reliable and realistic flux distributions are the prerequisites to the ROP analysis to derive the reactor trip set points.

Although the investigation should preferably be carried out by coping with local fluxes, it is here dealt with zonal fluxes by comparing the zonal flux tilts between zones and the change in tilts with model changes. This approach would be an appropriate method to grasp a more realistic glance on the effects of structural material mesh spacing layouts, and the method could be extended to the dealing with local fluxes at a later stage, e.g., vanadium detector fluxes (Ref. 10). In short, this kind of exercises would be beneficial to cope with the estimate of off-line flux mapping errors in context of BP/CP uncertainty analysis more realistically and reliably.

For zone *i* the zonal flux tilt is defined as follows;

$ZFT_{i,j}$ (%) = $(ZF_j-ZF_i)/(ZF_j+ZF_i)*100$, $i=1$ *to* 13 and $j=i+1$ *to* 14.

The zonal flux ZF_i is the volume integrated average flux in zone *i*. In Table 7 $ZFT_{i,j}$ are given for Model R.

The tilts associated with zone # 2,9 and 3,10 show relatively larger values of the tilts compared to the other zones. The zonal flux tilts for the very top and bottom zones, namely, $ZFT_{3,5}$, $ZFT_{3,12}$, $ZFT_{5,10}$ and $ZFT_{10,12}$ are all less than 1% in its absolute values.

Note that for $ZFT_{i,j}$, for $i=1$ *to* 7 and $j=i+7$, the absolute values of tilts are less than 0.1% which vindicate the balanced convergence on the axial irradiation shape, and the axial power distribution is symmetric. The number of the absolute values of $ZFT_{i,j}$ out of the total 91 values that is larger than 4% is 56. And this is more than half of the total numbers. By adjusting and optimizing the exit burnup distribution in each buenup zone this number could be possibly reduced.

Table 7 Zonal Flux Tilts $ZFT_{i,j}$ (%) for Model R

	Zone j												
Zone i	*i+1*	*i+2*	*i+3*	*i+4*	*i+5*	*i+6*	*i+7*	*i+8*	*i+9*	*i+10*	*i+11*	*i+12*	*i+13*
1	-0.51	13.42	6.69	12.74	0.90	0.37	0.08	-0.60	13.49	6.68	12.66	0.93	0.32

2	13.93	7.20	13.25	1.41	0.88	0.59	-0.09	13.99	7.19	13.17	1.44	0.83
3	-6.79	-0.69	-12.54	-13.06	-13.35	-14.02	0.07	-6.80	-0.77	-12.51	-13.11	
4	6.10	-5.80	-6.32	-6.61	-7.29	6.86	-0.01	6.02	-5.77	-6.37		
5	-11.86	-12.38	-12.67	-13.34	0.76	-6.11	-0.08	-11.83	-12.43			
6	-0.53	-0.82	-1.50	12.61	5.79	11.78	0.03	-0.58				
7	-0.29	-0.98	13.13	6.31	12.30	0.56	-0.05					
8	-0.68	13.41	6.60	12.59	0.85	0.24						
9	14.08	7.28	13.26	1.53	0.92							
10	-6.87	-0.84	-12.58	-13.18								
11	6.03	-5.76	-6.37									
12	-11.75	-12.35										
13	-0.61											

9. Standard Deviation of Zonal Flux Tilts

Considering the fact that Model R given here could be presently claimed as the most precise RFSP-IST core model for CANDU 6 reactor with respect to the effects of structural material mesh spacing layouts, it is felt worthwhile to weigh the quality of the other models, namely, Models A-G and S, and it is done so by introducing the standard deviation of the zonal flux tilts of these models compared to Model R. For this purpose, the error of zonal flux tilt is defined as follows;

ε (%) = $(ZFT_{i,j,\mathrm{Model\ A\text{-}G,S}}/ZFT_{i,j,\mathrm{Model\ R}} - 1)\mathrm{x}100$, *i=1 to 13* and *j=i+1 to 14*.

The results of the comparisons are given in Table 8 where two sets of displays are merged in one table. The left display is based upon 91 zonal flux tilt values for each model and the last column, # (|ε|>σ), gives the number of zonal flux tilt errors whose absolute value is greater than the standard deviation value.

Table 8 Zonal Flux Tilt Average Errors ε and Standard Deviations σ

Model	Avg ε (%)	σ (%)	# (│ε│>σ)	Model	Avg ε (%)	σ (%)
A	0.34	1.74	11	**A**	-0.06	0.49
B	0.61	6.04	12	**B**	0.57	1.39
C	3.26	15.91	16	**C**	0.72	2.83
D	8.57	54.81	16	**D**	1.54	9.70
E	-21.76	66.91	12	**E**	-0.36	13.98
F	-21.61	63.71	12	**F**	-1.06	14.66
G	-19.05	78.17	12	**G**	5.12	18.92
S	-13.86	112.25	8	**S**	-0.16	42.76

Note that the average errors for two groupings of Models A-D and Models E-G,S show the opposite signs and the change in the absolute values of these errors also in the opposite direction. It is here again confirmed that neglecting the mesh lines in x-direction associated with the structural materials in RFSP-IST core model leads to significant departure of the flux distribution from the reference one.

In order to have different view of the comparisons, the zonal flux tilt errors whose absolute values are greater than the standard value are treated as irrational and removed from recalculating zonal flux tilt errors and standard deviations. The results so obtained are shown on the right area of Table 8. As expected the values of the average zonal flux tilt errors and standard deviations are much dampened and the monotonic increase in standard deviations for Models E-G,S can be observed in contrast to the left area display in Table 8.

10. Conclusions

In the present paper, the effects of structural material mesh spacing layouts for CANDU 6 reactors are assessed by creating models with and without inclusion of mesh lines in x- and y-directions associated with the structural materials of core model. For this purpose the most precise Model R, 60x98x40 mesh volumes, is set up and used as the reference model to measure the quality of other models that are set up by neglecting optionally the mesh lines associated with the structural materials.

Neglecting the mesh lines associated with the structural materials in x-direction lead to relatively more noticeable change, degrading in the accuracy of zonal flux distributions, compared to the case of y-direction mesh lines. Thus, it is strongly suggested that the mesh lines in x-direction of core model associated with the structural materials should be accounted for without any discarding.

Model R could be accepted as practically affordable model in terms of computing time and should be qualified for the use to estimate BP/CP uncertainty of Wolsong CANDU 6 reactors with respect to the derivation of uncertainty values for all 380 channels individually where the accurate local flux distributions are the prerequisites for the successful application of methodologies being prospected for the analysis works. This claiming would be more credited in consideration of off-line flux mapping errors that are the directly affected products by the precursory contribution of local flux shape uncertainties while the fundamental flux mode is calculated using the RFSP-IST determined instantaneous flux distributions.

The results produced and observations taken in the present study open doors to the subjects of establishing the systemized bias structure of errors additionally introduced into the flux distributions generated by using a RFSP-IST core model that is set up with the optional discarding of mesh lines associated with the structural materials. For a given model the above-mentioned bias could be established by using Model R. The interception of flux distributions by applying the systemized bias structure for a given core model should be justifiably exercised for such important core physics analysis as BP/CP uncertainty and ROP reactor trip set point analysis.

11. References

[1] D. Altiparmakov, "New Capabilities of the Lattice Code WIMS-AECL", Proc. Int. Conf. on Reactor Physics, Nuclear Power: A Sustainable Resource, PHYSOR-2008, Interlaken, Switzerland, September 14-19, 2008.

[2] G. Marleau, A. Hebert, and R. Roy, "A User Guide for DRAGON", Report IGE-174, Rev.5, École Polytechnique de Montréal , April 2000.

[3] B. Rouben, "RFSP-IST, The Industry Standard Tool Computer Program for CANDU Reactor Core Design and Analysis", Proceedings of the 13th Pacific Basin Nuclear Conference, Shenzhen, China, Oct. 21-25, 2002.

[4] D.B. Miller and E.S.Y. Tin, “POWDERPUFS-V User’s Manual”, AECL Report TDAI-31 Part 2, 1976 March.

[5] A.R. Dastur et al., “MULTICELL User’s Manual”, AECL Report TDAI-208, 1979.

[6] “CANDU Type Pressurized Heavy Water Reactor Nuclear Power Plant Standard Technical Specification Guidelines”, Prepared by Atomic Creative Technology Co., Ltd., October 2009.

[7] D.H. Chung, B.G. Kim, S.M. Kim, H.B. Suh, H.S. Kim and H.J. Kim, “Experience with Wolsong-1 Phase-B Pre-Simulations using WIMS/DRAGON/RFSP-IST Code Suite”, 31st Annual CNS Conference, Montreal, QC, Canada, May 24 - 27, 2010.

[8] T. Liang, W. Shen, E. Varin and K. Ho, “Improvement and Qualification of WIMS Utilities”, 29th Annual CNS Conference, Toronto, Ontario, June 1 - 4, 2008.

[9] M. Dahmani, “Qualification and Development Plan for the T16MAC Version 1.0”, AECL Report 153-113190-PLA-002, Rev. 0, 2007 November.

[10] H.J. Kim, D.H. Chung, J.H. Kim and S.M. Kim, “A Preliminary Study on BP/CP Uncertainty Analysis of Wolsong CANDU 6 Reactors Based Upon RFSP-IST Fine Mesh Core Model”, Paper to be presented, 32nd Annual CNS Conference, Niagara Falls, Ontario, Canada, June 5-8, 2011.